Applied Scientific Research **53:** 339–355, 1994.

© 1994 *Kluwer Academic Publishers. Printed in the Netherlands.*

A Comparison of Different Analytical Techniques for Identifying Structures in Turbulence

N.K.-R. KEVLAHAN[1], J.C.R. HUNT[1,2] and J.C. VASSILICOS[1]
[1] *DAMTP, University of Cambridge, U.K.*
[2] *Meteorological Office, Bracknell, U.K.*

Received 8 September 1993; accepted in revised form 4 April 1994

Abstract. Vortical structures play an important role in the kinematics and dynamics of turbulence, but in order to understand this role we require techniques to identify and classify them. Proper Orthogonal Decomposition (POD), conditional sampling with ensemble statistics, and conditional sampling with conditional statistics are applied to a simple test function and the results are compared to determine the strengths and weaknesses of each approach. The second method gives the closest approximation to the test signal and is the easiest to use, although it is sensitive to the choice of conditions. None of these techniques can give much insight into the dynamics of turbulence, or into the organisation of eddies with complex, fine-scale structure.
New methods for investigating complex (self-similar) structures based on fractal and wavelet analyses are presented. Methods of distinguishing between locally (accumulating) and globally (fractal) self-similar structures are suggested.

1. Introduction

There has been much interest recently in the identification of characteristic structures in turbulence as a way of understanding its dynamical properties such as intermittency, the transfer of energy between length scales and the dispersion of contaminants. Experiments and Direct Numerical Simulations (DNS) have provided evidence that turbulence is not random, but contains structures with complex internal organisation (Vincent and Meneguzzi, 1991). Statistical approaches to turbulence are capable of predicting some quantities averaged over many realisations of a turbulent flow, but they are not able to provide insight into dynamical quantities that are directly related to the flow structures of a given realisation. In order to be effective the structural approach requires mathematical tools capable of unambiguously identifying complex turbulence structures according to appropriate kinematical and dynamical criteria. Once different sorts of structures have been identified it is possible to determine which of them play important roles in the dynamics of turbulence.

Many mathematical techniques have been used to identify and describe structures, e.g. the Fourier transform, Karhunen–Loeve orthogonal decomposition (Lumley, 1967; Aubry et al., 1988), functional/pattern recognition (Mumford, 1982), non-functional conditional sampling (Hussain, 1986), kinematic classification (Chen et al, 1990; Kevlahan, 1992; Wray and Hunt, 1990), and, more recently, fractals (Vassilicos and Hunt, 1991) and the wavelet transform (Brasseur

and Wang, 1992; Farge, 1992; Hunt et al., 1993). Each of these techniques breaks down the flow in different ways and places a different emphasis on the various aspects of turbulence (usually velocity, pressure, and their gradients). The question then arises: which methods are best able to detect, classify and describe eddy structures which may contain significant complexity? This paper has two parts: the first is concerned with the identification and eduction of large coherent structures. The second presents and discusses subtler tools capable of identifying small scale complex eddy structure.

We evaluate three common eduction techniques for coherent structures, namely Proper Orthogonal Decomposition (POD), conditional sampling with ensemble statistics, and conditional sampling with conditional statistics by applying each of these techniques to a simple test function that is asymmetric and whose energy is not contained in a single mode (i.e. $f(x) = (a + xb)\exp-(x^2)$). Then we assess the strengths and weaknesses of each approach. Some of these techniques have been tested before on actual turbulent flows (e.g. Guezennec, 1989), but the goal here is to assess these techniques on mathematically simple test signals so that the precise differences between the techniques are brought out. Differences between the techniques and the reasons for those differences may be obscured when they are applied to more complex flows. The results show that these techniques can lead to quite ambiguous and erroneous inferences as to the structure of eddies.

In the second part of this paper we address the problem of identifying and analysing eddies with significant internal complexity; none of the traditional approaches described above are capable of giving this sort of information. By 'complex structure' we mean eddies with a self-similar or singular internal structure. The usual Fourier transform can provide some limited information about the existence of such singular regions or structures in the flow. A non-integer power law energy spectrum (e.g. Kolmogorov's $E(k) \propto k^{-5/3}$ for the inertial range of isotropic turbulence) implies that the velocity field must contain singularities 'worse' than discontinuities (Moffat, 1984; Hunt and Vassilicos, 1991; Zel'dovich and Sokolov, 1985). These singular structures could be cusps, accumulating discontinuities or oscillations (e.g. functions of the form $f(x) = x^s \sin(x^{-t})$), fractal functions (e.g. the non-differentiable Weierstrass function $f(x) = \sum_{k=1}^{\infty} \lambda^{(s-2)k} \sin(\lambda^k x)$), or some more complex superposition of these. Both the accumulating and fractal functions are self-similar, however the accumulating functions are self-similar only about a specific point while fractals (characterised by a non-integer Hausdorff dimension) are self-similar everywhere. Accumulating and fractal structures may be considered globally and locally self-similar respectively. Turbulence models have been developed using both these types of structures as building blocks (e.g. the fractal β-model of Frisch et al. (1978) and the strained spiral vortex model of Lundgren (1982)).

To detect whether or not the structure of eddies actually corresponds to that assumed by these models requires a method for unambiguously determining and distinguishing between global and local self-similarity. The differences between

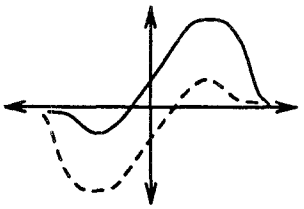

Fig. 1. Typical eddy structure from the test function $u(x) = (a + bx)\exp(-x^2)$.

these classes of self-similar structures are investigated by applying Fourier, wavelet and fractal methods to an accumulating test function as $f(x) = \sin 2\pi/x^t$ (which is locally self-similar) and a related function constructed from the random superposition of its Fourier components (which is globally self-similar). Finally, general analytical methods of distinguishing between locally and globally self-similar structures are proposed.

2. Comparison of Methods for Large Eddy Eduction

In this section we investigate the relative strengths and weaknesses of methods for eduction based on unconditional, or ensemble, statistics compared to those based on conditional sampling by applying each of them in turn to a simple one-dimensional test function.

Methods based on invariants of the deformation tensor and/or pressure (e.g. Wray and Hung, 1990; Chen et al., 1990) are in a different class, since unlike the above approaches they classify each point of the flow in a given realisation and do not extract whole eddy structures. Invariant/pressure methods do, however, have the advantage of being equally applicable to both large and small scale coherent structures. The invariant/pressure approach also requires more sophisticated and physically realistic test signals for evaluation, and for this and the previous reasons these methods are not included in the comparison.

The test function $u(x)$ we use is a simple sum of the Gaussian profile and its first derivative, both having random amplitudes, viz.:

$$u(x) = (a + bx)\exp(-x^2) \tag{2.1}$$

where a and b are normally distributed random variables with zero mean. This is representative of the velocity profile across a flow (e.g. a free shear flow) in which there are different kinds of eddies that are asymmetrical about the centre line $x = 0$ (see Fig. 1). If the eddies are uncorrelated with each other a and b are also uncorrelated. It is assumed that the variances σ_a^2, σ_b^2 of a and b are of similar magnitude. Each of the structure eduction techniques will be judged on its ability to pick out these typical eddies with the least amount of subjective manipulation. This is a more demanding task than in many flows, where the dynamics leads to a selection of a few dominant modes or types of eddy (Hussain, 1988).

2.1. Proper Orthogonal Decomposition (POD)

POD decomposes a signal onto a basis of non-specified functions chosen to represent the energy of the signal in the fewest number of modes. This method is completely objective (no possibility of subjective bias or control in the process), and it optimally efficient. The attempt to find the structure that is best correlated (in terms of energy) with the random turbulence field reduces to a problem of maximisation (Aubry et al., 1988). The calculus of variations reduces this maximisation problem to the solution of a Fredholm integral equations of the first kind

$$\int R_{ij}(x,x')\phi_j(x')\,\mathrm{d}x' = \lambda\phi_i(x), \tag{2.2}$$

where $R_{ij}(x,x')$ is the autocorrelation tensor and $\phi_i(x)$ are the eigenfunctions, or modes (which are often interpreted as independent eddy structures). Then the signal $u_i(x)$ may be written as the sum of the eigenfunctions $\phi_i^{(n)}(x)$ with random amplitudes $a^{(n)}$

$$u_i(x) = \sum_{n=1}^{\infty} a^{(n)}\phi_i^{(n)}(x). \tag{2.3}$$

The turbulent kinetic energy is the sum over the n eigenvalues

$$E = \int \langle u_i u_i\rangle\,\mathrm{d}x = \sum_{n=1}^{\infty}\lambda^{(n)}, \tag{2.4}$$

because of the orthogonality of the eigenfunctions and the statistical independence of the amplitudes, i.e.

$$\int \phi^{(n)}\phi^{(m)}\,\mathrm{d}x = \delta_{nm} \quad \text{and} \quad \langle a^{(m)}a^{(n)}\rangle = \delta_{mn}\lambda^m, \tag{2.5}$$

where $\langle\ \rangle$ denotes the ensemble average. In the case of discrete data, solving Eq. (2.2) reduces to a matrix inversion problem. Note that although (2.3) converges optimally fast, some signals require many POD modes to capture a significant portion of the energy. POD is only useful for those signals where the energy can be captured in a few modes, or where the coefficients $a^{(n)}$ decrease abruptly after a certain mode.

The correlation function of the test signal (2.1) is

$$R(x,x') = (\sigma_a^2 + \sigma_b^2 xx')\exp(-x^2 - x'^2), \tag{2.6}$$

where a and b are taken to be random uncorrelated variables with standard deviations σ_a and σ_b. For this simple correlation function Eq. (2.2) can be solved analytically by the separable kernel method (Arfken, 1985, p. 872) to give

$$u(x) = a^{(1)}\phi^{(1)}(x) + a^{(2)}\phi^{(2)}(x), \quad a^{(1)} = a^{(2)} = \sqrt{\pi}\,(\sigma_a^2 + \sigma_b^2) \tag{2.7}$$

where the two modes are symmetric and anti-symmetric,

$$\phi^{(1)} = \sqrt{2}\,\pi^{-1/4} x \exp(-x^2), \quad \phi^{(2)} = \pi^{-1/4} \exp(-x^2). \tag{2.8}$$

Note that neither $\phi^{(1)}$ nor $\phi^{(2)}$ describes the asymmetrical form of the general eddy (see Fig. 1). It is evidently misleading to interpret the largest mode, $\phi^{(1)}$, as a typical eddy of the flow. The problem of interpreting the first mode arises here because the energy of the signal is fairly evenly distributed between the two largest modes. If the majority of the energy is not captured by the first mode it is more appropriate to consider the truncated series $\sum_{n=1}^{N} a^{(n)} \phi_i^n$ for which an increase of N by 1 results in little increase in energy, but for which a decrease of N by 1 removes a large portion of the energy. The first N modes together are then interpreted as the typical flow structure. It is important to remember that signals are possible for which even this method of interpreting the POD is not suitable (e.g. the complex eddies studied in Section 3).

2.2. Conditional Sampling with Ensemble Statistics

The goal in conditional sampling is to estimate $\mathbf{u}(\mathbf{x}, t)$ given that the velocity at $(\mathbf{x}', t)$ assumes a specific value $\mathbf{u}(\mathbf{x}', t)$. It can be shown (see Adrian et al., 1988) that the best estimate of the profile $\mathbf{u}(\mathbf{x}, t)$, which is defined as $\hat{\mathbf{u}}(\mathbf{x})$, is the *conditional average*

$$\hat{\mathbf{u}}(\mathbf{x}) = \langle \mathbf{u}(\mathbf{x}, t) \mid \mathbf{u}(\mathbf{x}', t) \rangle. \tag{2.9}$$

The conditional average (2.9) can be approximated in terms of second-order (linear) and third-order (non-linear) two-point spatial correlations by

$$\hat{u}_i(\mathbf{x}) \sim A_{ij}(\mathbf{x}', \mathbf{x}) u_j(\mathbf{x}') + B_{ijk}(\mathbf{x}', \mathbf{x}) u_j(\mathbf{x}') u_k(\mathbf{x}') + O(u^3(\mathbf{x}')), \tag{2.10}$$

where A_{ij} and B_{ijk} are found by requiring that the mean-square errors $e_i = \langle (\hat{u}_i(\mathbf{x}) - u_i(\mathbf{x}))^2 \rangle$ be minima. Setting the derivatives of e_i with respect to A_{ij} and B_{ijk} equal to zero and carrying out the indicated averages gives the following equations for the components of A_{ij} and B_{ijk} for inhomogeneous, anisotropic turbulence

$$A_{ij}(\mathbf{x}', \mathbf{x}) \langle u_j u_l \rangle (\mathbf{x}') + B_{ijk}(\mathbf{x}', \mathbf{x}) \langle u_j u_k u_l \rangle (\mathbf{x}') = \langle u_l(\mathbf{x})' u_i(\mathbf{x}) \rangle \tag{2.11}$$

$$\begin{aligned} &A_{ij}(\mathbf{x}', \mathbf{x}) \langle u_j u_l u_m \rangle (\mathbf{x}') + B_{ijk}(\mathbf{x}', \mathbf{x}) \langle u_j u_k u_l u_m \rangle (\mathbf{x}') \\ &\quad = \langle u_l(\mathbf{x}') u_m(\mathbf{x}') u_i(\mathbf{x}) \rangle. \end{aligned} \tag{2.12}$$

In the case of homogeneous, isotropic turbulence these relations simplify to

$$A_{ij}(\mathbf{x}', \mathbf{x}) = \langle u_j(\mathbf{x}') u_i(\mathbf{x}) \rangle / u^2, \tag{2.13}$$

$$B_{ijk}(\mathbf{x}', \mathbf{x}) = 3\langle u_j(\mathbf{x}')u_k(\mathbf{x}')u_i(\mathbf{x})\rangle/2Ku^4 \tag{2.14}$$

where $u^2 = 1/3\langle u_i u_i\rangle$, and K is the kurtosis. Note that these correlations are *unconditional*, and they are not selected for particular 'eddies'; they are ensemble statistics. The Linear Stochastic Estimation (LSE) for $\mathbf{u}(\mathbf{x}, t)$ retains only the first term on the right-hand side of Eq. (2.10).

From (2.10), (2.11), and (2.12) the LSE for our test function is

$$u(x) = \frac{R(x, x')}{\langle u^2(x')\rangle}\, u(x'), \tag{2.15}$$

which, using (2.6), becomes

$$\hat{u}(x) = \frac{(\overline{\sigma_a^2} + \overline{\sigma_b^2} x x')\exp(-x^2 + x'^2)}{(\sigma_a^2 + \sigma_b^2 x'^2}\, u(x'). \tag{2.16}$$

This purely statistical estimate may be combined with conditional sampling to determine the form of all eddies whose maximum amplitude is negative, i.e. $u_{mx} < 0$. Conditional sampling governs how the reference point (in space and time) is chosen. In general, conditions are placed on both the location of the reference point, x', and the value of the velocity at that point, $u(x')$. If the location of the maximum (x_{mx}) is taken as the reference point x' then (2.16) shows that if $u_{mx} < 0$ the point $u = 0$ lies at $x = -\sigma_a^2/(\sigma_b^2 x')$. Therefore the location of the 'zero point' always has the opposite sign to that of the location of u_{mx}. This is a significant improvement over POD: the conditional eddy correctly represents the qualitative characteristics of the typical physical eddy as shown in Fig. 1.

How robust is the conditional eddy to changes in the sampling criteria? Consider a purely conditional approach (not based on the correlation tensor). If the conditional average is based on the criterion $x_{mx} > 0$ then the conditional eddy becomes

$$\langle u(x)^2 \mid x_{mx} > 0\rangle = \sigma_b^2 x \exp(-x^2). \tag{2.17}$$

This conditional eddy has lost all information about the symmetrical part of the velocity field (and half the energy)! If we now add an additional criterion $u(0) > 0$ the conditional eddy becomes

$$\langle u(x)^2 \mid x_{mx} > 0, u(0) > 0\rangle = (\sigma_a^2 + \sigma_b^2)\exp(-x^2). \tag{2.18}$$

This is again a very different structure from the one obtained by conditioning only on $x_{mx} > 0$. These examples show how sensitive the LSE method can be to the conditions chosen: slight changes in conditions can lead to the identification of completely different eddies.

2.3. Conditional Sampling and Conditional Statistics

The Coherent Structures method (Hussain, 1986) is an interactive and iterative from of conditional sampling. In this approach one first defines the signal, its nature and the relevant length scales of the coherent structure for there to be a conditional event. The location of the structure is adjusted until an optimal mean structure pattern is obtained. If the spread of structures is too great one reclassifies, introducing more structure classes. This process continues until an optimal mean structure pattern with minimum spread is obtained.

Consider our test signal (2.1). Initially we may decide that there is only one coherent structure, and then filter the signal to remove white noise. On examining the signal we could then split the structures into two classes based on the sign of the maximum velocity: $u_{mx} > 0$ and $u_{mx} < 0$. This classification would still allow too great a spread of structures so we would reclassify further into four groups based on the sign and position of the maximum velocity: $u_{mx} > 0$, $x_{mx} > 0$, $x_{mx} < 0$, $u_{mx} < 0$, $x_{mx} > 0$, $u_{mx} < 0$, $x_{mx} < 0$. These structure classes can be further divided by the magnitude of the maximum velocity: e.g. $1/2 < u_{mx} < 1$, $1 < u_{mx} < 3/2$, $3/2 < u_{mx} < 2$, $2 < u_{mx} < 5/2$, $5/2 < u_{mx}$. Finally, by this iterative, subjective process we have ended up with twenty structure classes. This example shows that the coherent structures approach can require a large amount of manipulation to obtain representative structures, but also permits a great deal of fine control and sensitivity. An advantage of this approach is that, unlike LSE, it is able to separate out the incoherent noise of the signal.

3. Small Scale Complex Eddy Structures

How can small scale structures with complex internal organisation (e.g. the accumulating oscillatory signal from a cut through a spiral vortex) be identified? The continuous spectrum and accumulating structure of these eddies makes them difficult to represent in a few terms of a series (their energy is not concentrated in the first few POD modes). Conditional sampling is also inappropriate since it is difficult to extrapolate on such a highly oscillatory function. New tools are definitely needed to identify and analyse eddies with complex fine scale structure.

In this section we introduce some new tools for the analysis of complex eddy structures and apply them to two test signals: a $\sin(2\pi/x)$ 'spiral' which is an oscillatory locally self-similar function, and the Fourier phase scrambled version which is a globally self-similar fractal function. We use two new tools: the box-counting algorithm and the wavelet transform, and one old tool: the Fourier transform. The problem we address here is how to determine whether turbulence has a locally self-similar ('spiral') structure, or a globally self-similar fractal structure. The long term goal of the analysis of complex eddy structures is to find the relation between the quantities α (the exponent of the self-similar Fourier energy spectrum), $\phi(k)$ (the Fourier phase spectrum), D_K (the Kolmogorov capacity, a measure of

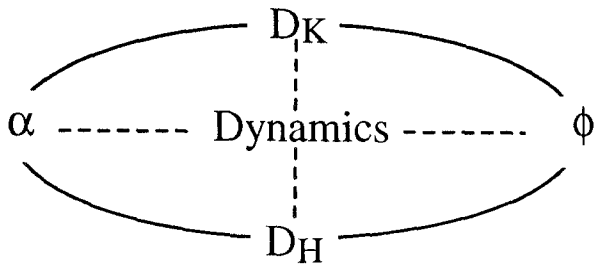

Fig. 2. The relation between quantities important for the analysis of the fine-scale structure of turbulence: the exponent of the Fourier energy spectrum α, Fourier phase spectrum $\phi(k)$, Kolmogorov capacity D_K, and Hausdorff dimension D_H. The solid lines indicate primarily fixed relationships, while the dotted lines indicate that the relationship is determined by the dynamics of the turbulence.

self-similarity), D_H (the Hausdorff dimension, a non-integer Hausdorff dimension defines a fractal) and the dynamics and geometry of the flow (see Fig. 2).

The box-counting algorithm gives a number (the Kolmogorov capacity) which characterises the self-similarity of a signal. A non-integer Kolmogorov capacity means that the signal is in some way self-similar, however both locally and globally self-similar functions will have a non-integer dimension. The Kolmogorov capacity alone cannot tell us whether the turbulence is fractal or spiral.

The general form of our accumulating 'spiral' test function

$$f(x) = x^2 \sin(2\pi x^{-t}) \tag{3.1}$$

is locally self-similar; its zero crossings form a set of points which Hausdorff dimension $D'_H = 0$, but a non-trivial Kolmogorov capacity $D'_K = t(t+1)$ (Hunt et al., 1993). Using the method of stationary phase, one finds that for large k the energy and phase spectra of (3.1) are given by (Hunt et al., 1993)

$$E(k) \propto k^{-2p} \tag{3.2}$$

$$2p = (2s+1)(1 - D'_K) + 1 \tag{3.3}$$

$$\phi(k) \propto k^{D'_K} \tag{3.4}$$

provided that $1 < 2p < 2$, $-t < s < 1$, and $t > 0$.

Orey (1970) showed that Gaussian sample functions with an energy spectrum $E(k) = k^{-2p}$ are fractal and that their zero crossings have a Hausdorff dimension

$$D'_H = \frac{1}{2}(3 - 2p). \tag{3.5}$$

Notice that the two functions just mentioned differ in three aspects: (i) $D'_H = 0$ for (3.1), $D'_H \neq 0$ in (3.5), (ii) they have different relations between p and respectively D'_K and D'_H, (iii) they have different phase spectra – the phase spectrum of a

Gaussian random function is random. A question which then arises is whether the *phase spectrum* can discriminate between local and global self-similarity.

To study the relation between an ordered phased spectrum $\phi(k)$ and the type of self-similar structure we took the Fourier transform of the accumulating function (3.1) with $s = 0$ and $t = 1$, scrambled the phases and then transformed back to physical space. This procedure destroys the spatial organisation of the original signal and produces a function that is quantitatively and qualitatively indistinguishable from a fractal in the Hausdorff sense. The Kolmogorov capacity of the signal was significantly altered by this operation! In fact it is then given by Eq. (3.5) for Gaussian random functions. This property appears to be generally true for power-law spectra with random phase (Osborne and Provenzale, 1989), but may not hold for practical reasons related to the scrambling procedure when $s \neq 0$ in the initial signal. By considering both the scrambled and original versions of the signal we will try to find analytical ways capable of distinguishing between such localised and global self-similar structures that we have the same energy spectra or Kolmogorov capacities, but different phase spectra and Hausdorff dimensions.

3.1. Box counting analysis and Kolmogorov capacity

The Kolmogorov capacity (D_K) of a curve is calculated by finding the slope on a log-log graph of the plot of the number of boxes required to cover the curve as a function of the size of the box. The range of length-scales which need to be resolved to calculate D_K is in certain cases much smaller than that required to obtain a good estimate of the exponent of the energy spectrum (Vassilicos and Hunt, 1991).

Thus, the Kolmogorov capacity is a more practical measure of self-similarity than the energy spectrum. Although D_K alone cannot distinguish between the original and scrambled signals, the overall shapes of the curves do differ significantly. In the case of the scrambled signal the transition from a slope of -1.5 (the true dimension of the function) to 0 (caused by the finite number of points in the representation of the function) is very abrupt, while in the case of the original signal the transition is much more gradual (see Fig. 4). This difference is due to the fact that in the original signal the points representing the function are distributed evenly, but the increasingly smaller scales emerge only as one near the origin. The scrambled signal is self-similar at every location, so the box-counting algorithm suddenly saturates everywhere at a particular length-scale whereas in the original signal the saturation occurs at different length-scales at different positions, thus smoothing the transition of the box-counting curve. This result may give a practical way of distinguishing between locally and globally self-similar structures.

The on-off function generated by the zero-crossings, i.e. the function that jumps from 0 to 1 and from 1 to 0 at the zero-crossings, but remains constant elsewhere, has a Fourier power spectrum $\Gamma(k) \sim k^{-2\rho}$, $2\rho = 2 - D'_K$ (Vassilicos and Hunt, 1991), whether the zero-crossings are of a fractal or a spiral signal. Two such different signals with the same value of D'_K will have the same ρ, but different p.

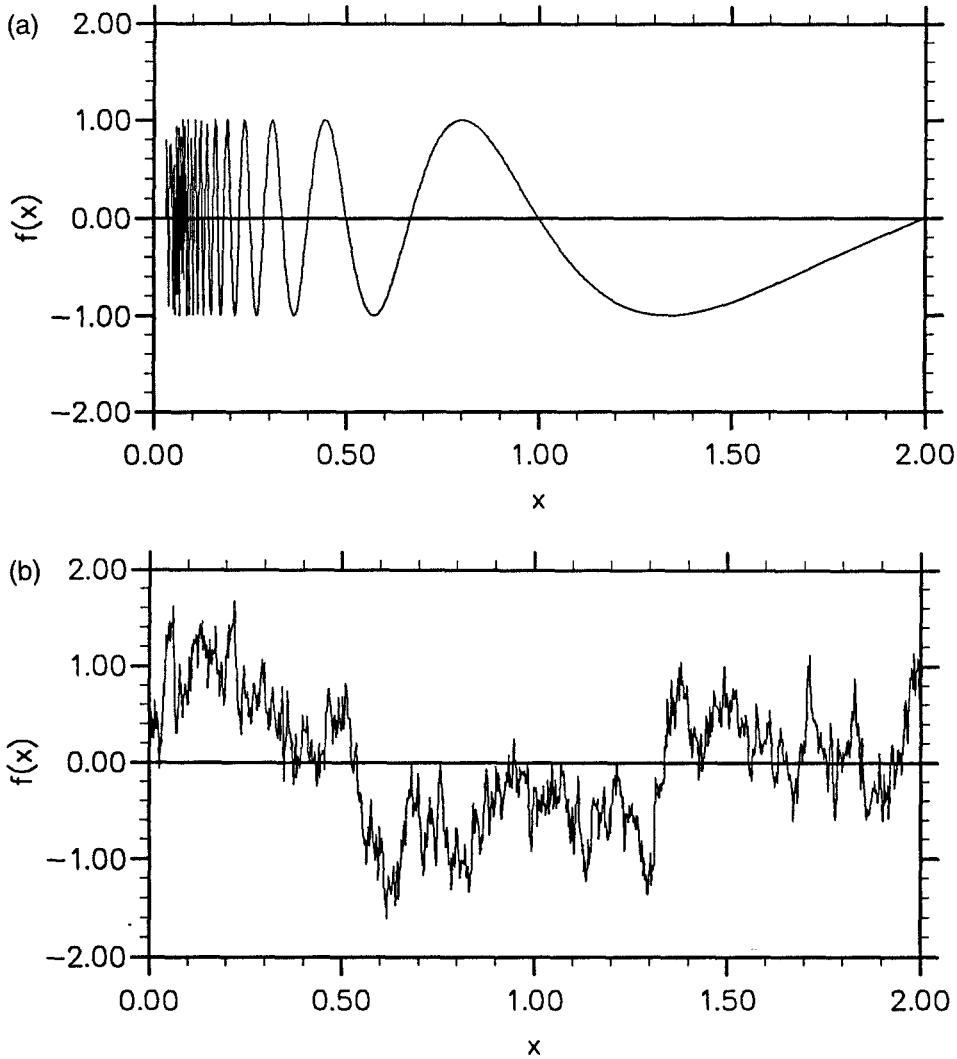

Fig. 3. (a) Original, and (b) scrambled versions of the accumulating function $f(x) = \sin(2\pi/x)$.

In the case of Gaussian sample functions, $p = 2\rho - 1/2$ (see (3.5)); in the case of spiral functions, such as (3.1), the relation between p and ρ is different. A good understanding of this relation may again lead to new practical ways of detecting whether $D'_H = 0$.

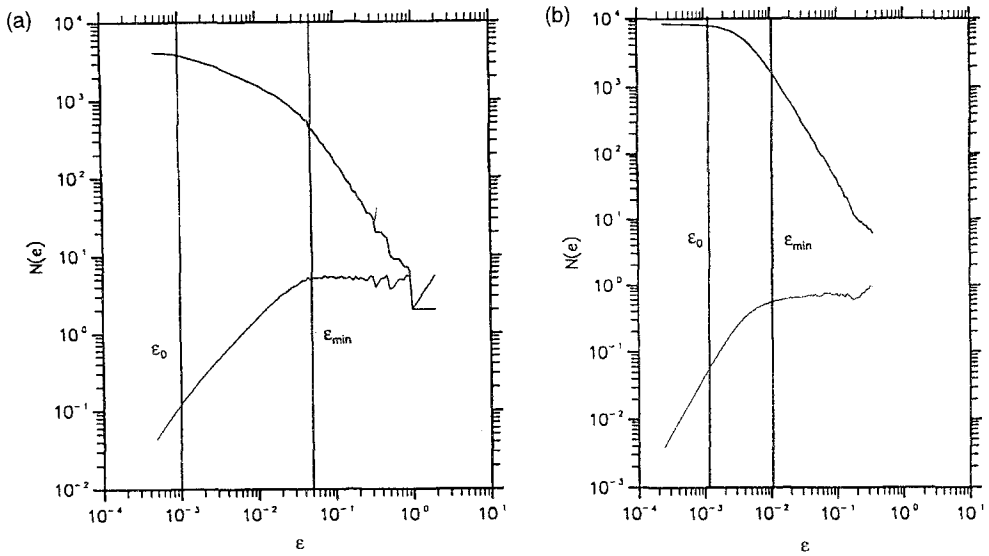

Fig. 4. Calculating the box-counting dimension. (a) Spiral function $\sin(2\pi/x)$, lower curve is $\times\varepsilon^{1.5}$. (b) Scrambled spiral, lower cure is $\times\varepsilon^{1.75}$. Note the much more gradual transition between $\varepsilon_{\min}$ (the lower limit of the power-law section of the curve) and ε_0 (the minimum spacing between points in the signal) for the locally self-similar spiral.

3.2. Wavelet Analysis

A more systematic tool for obtaining local information about spectral quantities is the recently developed wavelet transform (Grossman and Morlet, 1984; Farge, 1992)

$$\tilde{f}(\lambda, x_0) = \lambda^{-1/r} \int_{\infty}^{\infty} f(x)\psi^* \left(\frac{x - x_0}{\lambda}\right) \mathrm{d}x. \tag{3.6}$$

The wavelet transform allows one to investigate the structure of the signal $f(x)$ at different scales λ and different positions x_0 simultaneously. Because we are interested in what are essentially local fractal dimensions and fractal dimensions are related to energy spectra the wavelet transform would seem to be a good way of determining whether a flow contains locally self-similar accumulating functions or global fractal structures. In this section we use the wavelet analysis to develop another way of distinguishing between our locally and globally self-similar test functions.

Using the Morlet wavelet,

$$\psi(x) = e^{ik_g x} e^{-(|x|^2/2)}, \tag{3.7}$$

the squared modulus of the wavelet transform of the $\sin(2\pi x^{-t})$ spiral is

$$|\tilde{f}(\lambda, x_0)|^2 \sim \lambda^{1/2} \lambda^{-((2s+1)(D'_K-1)+1)} \exp\left[-\frac{(x_0 - (t\lambda)^{1-D'_K})^2}{2\lambda^2}\right], \tag{3.8}$$

where λ is the length-scale and x_0 is the location. The wavelet transform of the spiral is thus peaked around $x_0 = (t\lambda)^{1-D'_K}$. By contrast, the wavelet transform of the scrambled spiral shows no spatial organisation, although, of course, it reflects the overall distribution of the energy of the signal between different length-scales (see Fig. 5). This difference is brought out most clearly by looking at the local wavelet energy spectra at various locations. The local wavelet energy spectrum is obtained from the modulus of the wavelet transform by taking a slice through length-scale space at a particular location. The difference between the scrambled and spiral test functions is obvious in Fig. 5. The scrambled spiral has essentially the same local energy spectrum everywhere (on average $\propto k^{-((2s+1)(D'_K-1)+1)}$ where D'_K is the capacity of the original spiral), but the spiral test function has different ranges of $k^{-((2s+1)(D'_K-1)+1)}$ spectrum depending on the location. Looking at the way the local energy spectrum varies from position to position may provide another way of determining whether turbulence has a 'spiral' or fractal structure.

It has been claimed that branching in the wavelet transform indicates the signal is fractal (e.g. Arnéodo et al., 1989), however this is not necessarily the case. If a signal holds only one singularity of the type (3.1) and is totally regular elsewhere, then (3.8) shows that the wavelet transform will point towards $x_0 = 0$ since most of the power $|\tilde{f}(\lambda, x_0)|^2$ is concentrated around a curve $x_0 \sim \lambda^{1-D'_K}$ in the x_0–λ plane of the wavelet transform. The exponents t and s or D'_K and s characterising this singularity can be extracted from the examination of that curve and of the scaling of the wavelet transform along that curve. Problems arise when the signal carries an unknown distribution of singularities of the type (3.1), thereby producing a plethora of intertwined inverse branchings which may not be easily distinguishable from the branching pattern obtained when a fractal or multifractal signal is wavelet transformed (or even when random noise is transformed). It is then not a trivial task to untangle the local scaling exponents from the wavelet transforms of a complex signal, let alone interpret them. A simple example of the way this sort of fractal-like branching may arise is shown in Fig. 6.

Note also that one must be careful in applying real wavelet transforms to determine scaling exponents (related to Hausdorff dimension). Vergassola et al. (1991) have shown that spurious scaling exponents can be obtained from the Mexican Hat wavelet transform of a fractional Brownian signal. The same conclusion is reached, for other reasons, on the basis of a different example: the spiral accumulation function $\sin 2\pi x^{-t}$. From (3.8) it can be seen that the closer x_0 is to 0, the centre of the accumulation, the smaller the range over which $|\tilde{f}|^2$ is dominated by the power law $\lambda^{1/r}\lambda^{((2s+1)(D'_K-1)+1)}$ rather than by the Gaussian filter. A calculation of the scaling over the wrong range will give misleading results. Furthermore, even in the correct range, the detection of a power law does not prove that the signal is fractal; it can evidently also be a spiral accumulation. These two examples show the difficulty of determining the precise self-similar nature of a signal.

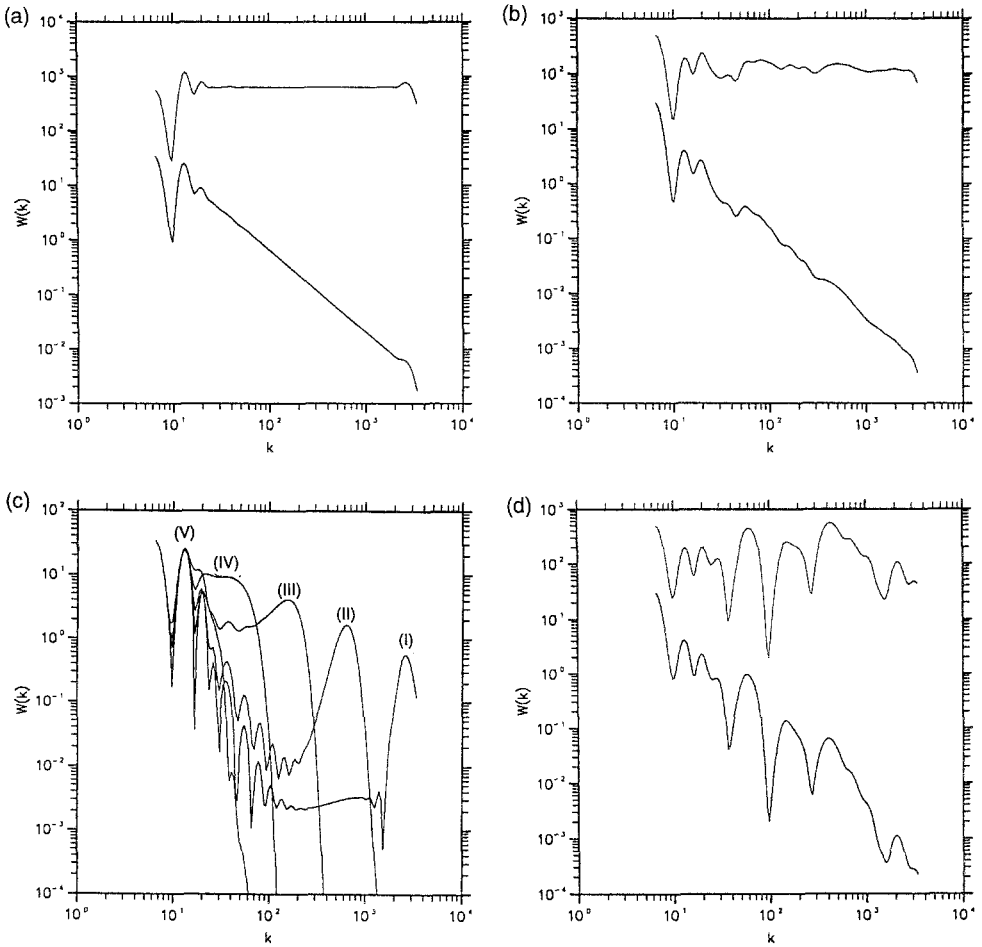

Fig. 5. Distinguishing between locally and globally self-similar signals using the wavelet transform. (a) Wavelet energy spectrum averaged over all locations for the spiral (upper curve is $\times k^{1.5}$). (b) Wavelet energy spectrum averaged over all locations for the scrambled spiral (upper curve is $\times k^{1.5}$). (c) Local wavelet spectra $\times k^{1.5}$ of the spiral at locations (I) 0.05, (II) 0.1, (III) 0.2, (IV) 0.4, (V) 0.8. The flat regions indicate the locations of $k^{-1.5}$ spectrum. (d) Typical local wavelet spectrum of the scrambled spiral at location $x = 0.4$ (upper curve is $\times k^{1.5}$).

4. Conclusions

By applying the POD, conditional sampling with conditional statistics (Linear Stochastic Estimation), and conditional sampling with conditional statistics (Coherent Structures) to a test signal we have clarified the strengths and weaknesses of each approach. First, the physical interpretation of POD is unclear: the first eigenmode will *not* be a typical flow structure unless it contains most of the energy. Secondly, conditional sampling can give a qualitatively accurate physical representation of

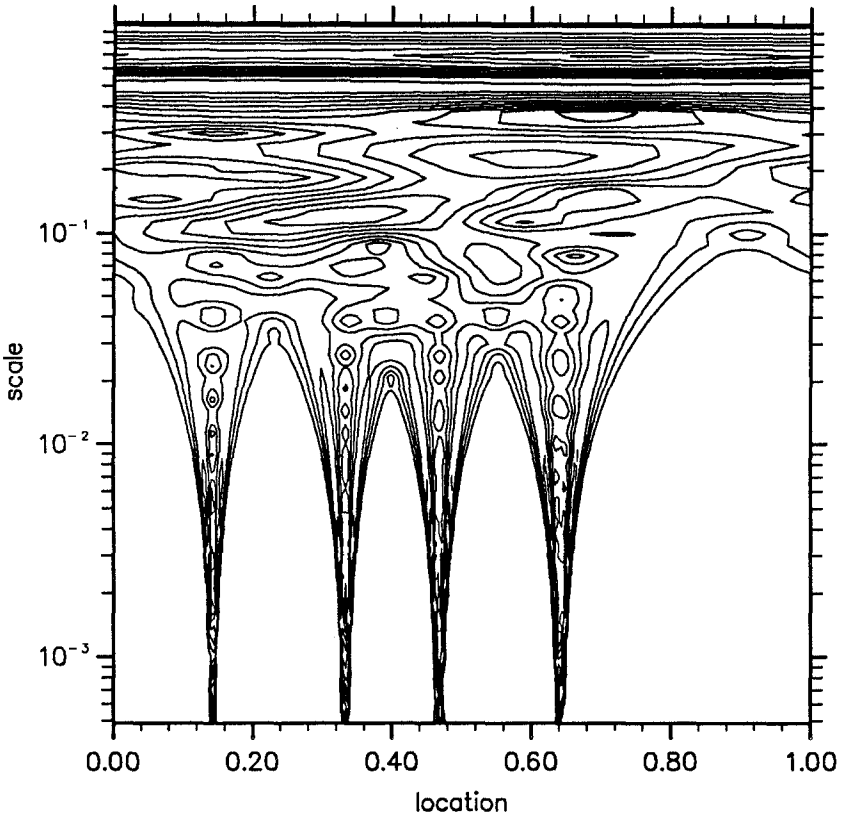

Fig. 6. Branching pattern in the modulus of the Morlet wavelets transform produced by a random superposition of four $\sin(2\pi/x)$ spirals.

the flow structures, but the resulting eddy may be sensitive to the precise conditions chosen. A combination of ensemble statistics with conditions determining the location (in space and time) of the reference point gives physically realistic results with a minimum of manipulation. Thirdly, the Coherent Structures method requires significant manipulation to obtain representative structures, although the interactive nature of this approach also makes it the most flexible and least liable to misinterpretation. The Coherent Structures approach also gives a way of separating out the incoherent noise of the signal.

Approaches based on invariants of the deformation tensor and pressure can give information about the relative number and location of regions with particular dynamics, but say nothing about their shape or internal structure. No clear way of interpreting invariant plots exists yet!

None of the above methods are incapable of analysing or identifying the local fine-scale structure of the flow.

The new techniques of fractal analysis and the wavelet transform have been applied to the problem of distinguishing between globally ('fractals') and locally

TABLE I. The differences between signals with random and non-random phase spectra

$\phi(k)$ random	$\phi(k)$ non-random
$D_H = D_K = \frac{1}{2}(5-\alpha)$	D_H, D_K, α – no fixed relation
– no energy cascade	– allows for cascade
– no structures	– allows for structures

('spirals') self-similar signals. The Kolmogorov capacity gives one parameter for describing the average degree of convolutedness within a coherent structure where the fields are self-similar over a range of length scales that may be quite small compared to those necessary for conventional Fourier methods. Alone among the methods examined, the wavelet transform is able to provide a simple functional description in terms of *local* length scales and position of the typically complex distribution of velocity and vorticity within turbulence structures. Three methods of distinguishing between fractals and spirals have been suggested: the first is based on the box counting algorithm (the variation of the range over which a Kolmogorov capacity is clearly defined), the second exploits the difference between the Fourier power spectrum of the original function and the on-off function obtained from the zero-crossings, and the third uses the variation of the local wavelet energy spectrum with position.

The long term goal of the development of new techniques to analyse complex structure is to clarify the relationship between the Fourier energy spectrum (exponent α), the Fourier phase spectrum ($\phi(k)$), the Hausdorff dimension (D_H), and the Kolmogorov capacity (D_K). This knowledge will have far-reaching implications for a deeper understanding of the dynamics of turbulence. A major part of this investigation is a study of the differences between signals with a non-random $\phi(k)$ ('spirals') and those with a random $\phi(k)$ ('fractals'). The phase spectrum of turbulence largely determines its dynamics and structure. For example, if the phases of a DNS are randomised the characteristic small-scale vortex tubes vanish. The nature of the energy cascade also depends crucially on the phase spectrum; in a velocity field with random phases there can be no net cascade of energy. The phase spectrum also changes the relationship between D_K and D_H. In a $\sin 1/x$ spiral $D_K = 1.5$ and $D_H = 1$, while if the phases of the spiral are scrambled $D_K = D_H = 1.75$. The fixed relation between D_H and α given by Orey's formula (3.5) holds for a Gaussian (random phase) signal. It is interesting to note that the Kolmogorov cascade in turbulence implies a non-random $\phi(k)$ which in turn means that D_H in turbulence is probably not given by (3.5), i.e. if $\alpha = 5/3$ then $D_H \neq 2.67$ in three-dimensional turbulence (contrast with results of Procaccia et al., 1991). Some differences between signals with random and non-random phases are summarised in Table I.

This investigation has helped to quantify the differences between the many methods of analysing a turbulent flow into turbulence structures, and has suggested optimum structure types for elucidating the dynamics of turbulence. The results obtained will give greater power and precision to the structural approach to understanding turbulence.

Acknowledgement

NKRK and JCV have been supported by British Gas during this work.

References

Adrian, R.J. and Moin, P., Stochastic estimation of organised turbulent structure: homogeneous shear flow. *J. Fluid Mech.* 190 (1986) 531–559.

Arfken, G., *Mathematical Methods for Physicists*. Orlando: Academic Press (1985).

Arnéodo, A., Argoul, F., Bacry, E., Elezgaray, J., Freysz, E., Grasseau, G., Muzy, J.F. and Pouligny, B., Wavelet transform of fractals. In *Wavelets and Some of Their Applications, Proceedings of the Conference held in Marseille-Luminy, June 1989* (1989).

Aubry, N., Holmes, P., Lumley, J.L. and Stone, E., The dynamics of coherent structures in the wall region of a turbulent boundary layer. *J. Fluid Mech.* 192 (1988) 115–173.

Brasseur, J.G. and Wang, O., Structural evolution of intermittency and anisotropy at different scales analysed using three-dimensional wavelet transforms. *Phys. Fluids A* 4(11) (1992) 2538–2554.

Chen, J.H., Chong, M.S., Soria, J., Sondergaard, R., Perry, A.E., Rogers, M., Moser, R. and Cantwell, B.J., A study of the topology of dissipating motions in direct numerical simulations of time-developing compressible and incompressible mixing layers. In: *Studying Turbulence using Numerical Simulation Databases – III. Proceedings of the 1990 Summer Program.* Stanford: CTR (1990).

Falconer, K., Fractal Geometry – Mathematical Foundations and Applications. John Wiley & Sons (1990).

Farge, M., The wavelet transform. *Ann. Rev. Fluid. Mech.* 23 (1992).

Frisch, U., Sulem, P.-L. and Nelkin, M., A simple dynamical model of intermittent fully developed turbulence. *J. Fluid Mech.* 87(4) (1978) 719–736.

Grossman, A. and Morlet, J., Decomposition of Hardy functions into square integrable wavelets of constant shape. *SIAM J. Math. Anal.* 15 (1984) 723–736.

Guezennec, Y.G., Stochastic estimation of coherent structures in turbulent boundary layers. *Phys. Fluids A* 1(6) (1989) 1054–1060.

Hunt, J.C.R., Kevlahan, N.K.-R., Vassilicos, J.C. and Farge, M., Wavelets, fractals and Fourier transforms: Detection and analysis of structure. In: *Wavelets, Fractals and Fourier Transforms: New Developments and New Applications, Proceedings of the IMA Conference at Newham College, Cambridge, December 16–18, 1990* (1993) (to appear).

Hunt, J.C.R. and Vassilicos, J.C., Kolmogorov's contributions to the physical and geometrical understanding of small-scale turbulence and recent developments. *Proc. R. Soc. Lond. A* 434 (1991) 183–210.

Hussain, A.K.M.F., Coherent structures and turbulence. *J. Fluid Mech.* 173 (1986) 303–356.

Lumley, J.L., The structure of inhomogeneous turbulent flows. In: A.K. Yaglom and U.I. Tatarsky (eds), *Proceedings of the International Colloquium on the Fine Structure of the Atmosphere and Its Influence on Radio Wave Propagation, Moscow, June 15–22, 1965.* Moscow: Nauka (1967) pp. 166–176.

Lundgren, T.S., Strained spiral vortex model for turbulent fine structure. *Phys. Fluids* 25(2) (1982) 2193–2203.

Moffatt, H.K., 1984, Simple topological aspects of turbulent vorticity dynamics. In: T. Tatsumi (ed.), *Turbulence and Chaotic Phenomena in Fluids.* Elsevier (1984) p. 223.

Mumford, J.C., The structure of the large eddies in fully developed turbulent shear flows. Part 1. The plane jet. *J. Fluid Mech.* 118 (1982) 241–268.

Orey, S., Gaussian sample functions and the Hausdorff dimension of a level crossing. *Z. Wahrscheinlichkeitstheory verw. Geb.* 15 (1970) 249.

Osborne, A.R. and Provenzale, A., Finite correlation dimension for stochastic systems with power-law spectra. *Physica D* (1989) 357–381.

Procaccia, I., Brandenburg, A., Jensen, M. and Vincent, A., The fractal dimension of isovorticity structures in 3-dimensional turbulence. NORDITA preprint, *Europhys. Lett.* (1991) (submitted).

Vassilicos, J.C. and Hunt, J.C.R., Fractal dimensions and the spectra of interfaces with applications to turbulence. *Proc. R. Soc. Lond. A* 435 (1991) 505–534.

Vergassola, M., Benzi, R., Biferale, L. and Pisarenko, D., Wavelet analysis of a Gaussian Kolmogorov signal. *Proceedings of the USA–French Workshop on 'Wavelets and Turbulence'* (1991).

Vincent, A. and Meneguzzi, M., The spatial structure and statistical properties of homogeneous turbulence. *J. Fluid Mech.* 225 (1991) 1–20.

Zel'dovich, Ya.B. and Sokolo, D.D., Fractals, similarity, intermediate asymptotics. *Sov. Phys. Usp* 28(7) (1985) 608–616.